Local-field effect on the linear optical intersubband absorption in multiple quantum wells

Ansheng Liu
Institute of Physics, University of Aalborg, DK-9220 Aalborg Øst, Denmark
(Received 18 May 1994)

Using a microscopic local-field formulation, the linear optical absorption of a multiple-quantum-well (MQW) structure associated with intersubband transitions is investigated. Taking as a starting point a fundamental self-consistent integral equation for the local field, the *p*-polarized electric-field distribution inside each quantum well in the MQW structure is studied. It is demonstrated that the local field is essentially determined from a set of linear algebraic equations. Within the infinite-barrier approximation with an effective well width, numerical calculations of the optical absorption spectra are presented for a $GaAs/Al_xGa_{1-x}As$ multiple quantum well for different parameters such as the two-dimensional (sheet) electron concentration, the angle of incidence, and the number of wells. The numerical results show that the local-field effect leads to a notable blueshift of the peak-position energy in the absorption spectra as the sheet density of the electrons is increased, and that for larger angles of incidence the electromagnetic interaction among quantum wells gives rise to a significant broadening of the absorption peak when the number of wells is sufficiently large.

I. INTRODUCTION

It is well known that quantum confinement of carriers in a semiconductor quantum well leads to the formation of discrete states in the conduction and valence bands. An optical intersubband transition within the conduction band involves the absorption of a photon causing an electron to be excited from one confined state to a higher confined state. Such transitions have been investigated experimentally by using inelastic light scattering techniques[1-3] and by a direct measurement of the optical absorption spectra.[4-8] A very large dipole oscillator strength and a narrow linewidth of the resonance peak in the absorption spectrum of a multiple-quantum-well (MQW) structure were reported.[4-8] In addition, one of the interesting aspects of these intersubband transitions in systems such as $GaAs/Al_xGa_{1-x}As$ MQW's (Refs. 7, 9, and 10) and $In_xGa_{1-x}As/Al_xGa_{1-x}As$ MQW's (Ref. 11) is the observation of a blueshift of the peak-position energy in the absorption spectra as the two-dimensional electron density is increased. Such a blueshift was interpreted as being due to the depolarization and band-filling effects by Ramsteiner *et al.*[10] Pinczuk and co-workers[9] suggested that this type of blueshift stems from the direct and exchange intersubband Coulomb interactions. More recently, Manasreh *et al.*[7] measured the optical absorption spectra of $GaAs/Al_{0.3}Ga_{0.7}As$ MQW samples at the temperature $T=5$ K as a function of the two-dimensional electron density. A significant blueshift (~ 24 meV) of the peak location in the spectra was observed when the surface density of the electrons was increased from 3.25×10^{11} to 2.29×10^{12} cm^{-2}. They claimed that, in order to describe quantitatively the results observed in their experiment, it is necessary to incorporate many-body corrections, depolarization, and excitonlike shifts in the nonparabolic anisotropic envelope-function approximation calculations.[7]

From a theoretical point of view, the resonance features in the optical excitation spectra (e.g., optical absorption spectra, Raman scattering spectra, and so on) of low-dimensional systems such as MQW and superlattice structures are related to collective excitations of the entire system. In previous treatments of the collective excitations in MQW and superlattice structures, the self-consistent-field formalism of Ehrenreich and Cohen[12] has usually been used. Based on this linear density response theory, various collective modes such as quasi-two-dimensional plasmons, intersubband plasmons, magnetoplasmons, and phonon-plasmon modes were investigated theoretically.[13-15] The intrasubband and intersubband plasmons have also been detected experimentally by inelastic light scattering techniques.[1] More recently, the Ehrenreich-Cohen density response theory has also been used to study the linear electromagnetic response of one-dimensional quantum wires[16] and quantum-dot arrays.[17] It is known, however, that although the exchange-correlation effects and the image-charge effect due to the dielectric mismatch can be conveniently incorporated in the Ehrenreich-Cohen self-consistent-field formalism, in this theory the electromagnetic interactions of the system are treated essentially in the electrostatic limit.[18] Therefore retardation effects associated with the electromagnetic coupling of the system are neglected in the density response theory. Such effects play an important role in the analysis of the optical reflection and transmission spectrum; in particular, of the angular dependencies of the reflection and transmission coefficients.

In the present paper, using a newly developed microscopic local-field formalism in which the retardation effects associated with the electromagnetic interaction are taken into account (for a review of this formalism, the reader is referred to Ref. 19), we investigate the linear optical absorption of a MQW structure in connection with intersubband transitions. It is shown that the local-field

effect in the MQW structure can lead to a notable blueshift of the peak location in the optical absorption spectra as the sheet electron density is increased. Also, we demonstrate that the electromagnetic interaction among quantum wells in the MQW structure can give rise to a significant change in the peak location, the linewidth, and the shape of the absorption peak when the number of wells is sufficiently large.

The paper is organized as follows. In Sec. II, starting with a self-consistent integral equation for the local field, we analyze the p-polarized electric-field distribution within each quantum well in a MQW structure. It is demonstrated that the local-field calculation essentially is to solve a set of linear algebraic equations. By using infinite-barrier wave functions some analytical results are obtained for the local-field calculation. In Sec. III, taking as a numerical example a $GaAs/Al_xGa_{1-x}As$ MQW structure, we calculate the optical absorption spectra for different parameters such as the sheet electron concentration, the angle of incidence, and the number of wells in the MQW structure. A discussion of the local-field effect on the optical absorption and of the importance of taking into account the electromagnetic coupling among quantum wells in the MQW structure is given.

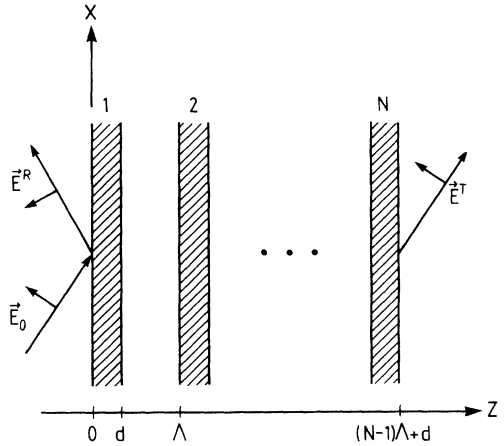

FIG. 1. Schematic diagram showing the reflection ($\mathbf{E}^R$) and transmission ($\mathbf{E}^T$) of a p-polarized incident field ($\mathbf{E}_0$) from a MQW structure having N wells. The shadowed areas represent the well layers. The thickness of each well layer is d, and the spatial period of the structure is Λ. The Cartesian xyz coordinate system used in describing the MQW system is also indicated.

II. THEORY

A. General result

Let us consider the case in which a monochromatic (a cyclic frequency ω) p-polarized plane wave is incident at an (internal) angle θ on a multiple-quantum-well structure consisting of N quantum wells embedded in an infinite medium with the relative dielectric constant $\epsilon^B(\omega)$. Described in a Cartesian xyz coordinate system, the surface normal of the structure points along the z axis, and the scattering plane is placed parallel to the xz plane, as illustrated in Fig. 1. Furthermore, let us assume that the barrier layer in the MQW structure is so thick that the overlap of the wave function of the electrons belonging to different quantum wells can be neglected. As a consequence, the electronic properties (wave functions and eigenenergies) of the MQW structure are determined essentially from a single quantum well. For simplicity, in this work we only consider the situation in which each quantum well in the MQW structure has only two bound states within the conduction band. Of these one is located above and the other below the Fermi level (ϵ_F) of the system. Thus, taking advantage of the translational invariance of the MQW system parallel to the well (xy plane), one realizes that the z-dependent local electric field $\mathbf{E}^{(n)}(z)$ within the nth quantum well is determined from the following inhomogeneous self-consistent integral equation:[19,20]

$$\mathbf{E}^{(n)}(z)=\mathbf{E}_0(z)-i\mu_0\omega\sum_{m=1}^{N}\int\int_{(m)}\vec{\vec{G}}(z,z')\cdot\vec{\vec{\sigma}}^{(m)}(z',z'')\cdot\mathbf{E}^{(m)}(z'')dz''dz' , \tag{1}$$

where the mark "(m)" under the integral symbol means that the integrations run over the mth quantum well. The first term on the right-hand side of Eq. (1), i.e.,

$$\mathbf{E}_0(z)=E_0(\cos\theta,0,-\sin\theta)e^{iq_\perp z} , \tag{2}$$

represents the incident field, where E_0 is the amplitude of the incident wave, and $q_\perp=\sqrt{\epsilon^B(\omega)(\omega/c_0)^2-q_\parallel^2}$ is the wave-vector projection perpendicular to the surface, $q_\parallel$ and c_0 being the parallel component of the wave vector and the light speed in vacuum, respectively. The tensor $\vec{\vec{\sigma}}^{(m)}(z',z'')$ appearing in Eq. (1) is the linear nonlocal conductivity response function of the mth quantum well. Within the random-phase approximation (RPA) and in the long-wavelength ($q_\parallel\to 0$) and low-temperature ($T\to 0$) limits, the linear conductivity response tensor takes a diagonalized form, and the relevant diagonal elements for a two-level quantum well are given by the following well-known expressions:[20–22]

$$\sigma_{xx}^{(m)}(z',z'')=\frac{ie^2}{\pi\hbar^2\omega}\frac{(\epsilon_2-\epsilon_1)(\epsilon_F-\epsilon_1)^2}{[\hbar(\omega+i/\tau)]^2-(\epsilon_2-\epsilon_1)^2}\times\phi^{(m)}(z')\phi^{(m)}(z'') , \tag{3}$$

$$\sigma_{zz}^{(m)}(z',z'')=\frac{ie^2}{2\pi m^*\omega}\frac{(\epsilon_2-\epsilon_1)(\epsilon_F-\epsilon_1)}{[\hbar(\omega+i/\tau)]^2-(\epsilon_2-\epsilon_1)^2}\times\Phi^{(m)}(z')\Phi^{(m)}(z'') . \tag{4}$$

In the equations above, ϵ_1 and ϵ_2 denote the eigenenergies of the two bound states (1 and 2) within the conduction

band, and τ is the relaxation time of the electrons associated with the intersubband transition between these two states. The charge and effective mass of the electrons are denoted by $-e$ and m^*, respectively. For brevity, we have also introduced the quantities

$$\phi^{(m)}(z)=\psi_1(z)\psi_2(z) , \tag{5}$$

and

$$\Phi^{(m)}(z)=\psi_1(z)\frac{d\psi_2(z)}{dz}-\psi_2(z)\frac{d\psi_1(z)}{dz} , \tag{6}$$

where $\psi_1(z)$ and $\psi_2(z)$ are the corresponding (real) wave functions of the eigenstates ϵ_1 and ϵ_2 of the mth quantum well. Note that in obtaining Eqs. (3) and (4) we have neglected the conduction-band nonparabolicity effect.

The retarded Green's function $\vec{\vec{G}}$ that enters Eq. (1) is given in dyadic form by[23,24]

$$\vec{\vec{G}}(z,z')=\frac{e^{iq_\perp|z-z'|}}{2iq_\perp}\times[\mathbf{e}_y\mathbf{e}_y+\Theta(z-z')\mathbf{e}_i\mathbf{e}_i+\Theta(z'-z)\mathbf{e}_r\mathbf{e}_r]+[\epsilon^B(\omega)]^{-1}\left[\frac{c_0}{\omega}\right]^2\mathbf{e}_z\mathbf{e}_z\delta(z'-z) , \tag{7}$$

where $\mathbf{e}_y=(0,1,0)$,

$$\mathbf{e}_i=(c_0/\omega)(q_\perp,0,-q_\parallel)/\sqrt{\epsilon^B} ,$$

and

$$\mathbf{e}_r=(c_0/\omega)(-q_\perp,0,-q_\parallel)/\sqrt{\epsilon^B}$$

are the relevant unit vectors, Θ is the Heaviside unit step function, and δ is the Dirac δ function. On the right-hand side of Eq. (7), the first term [proportional to $\exp(iq_\perp|z-z'|)$] is the direct propagating part (from z' to z) of the electromagnetic propagator, and the second term [proportional to $\delta(z'-z)$] is the so-called self-field part of the propagator.[24] Therefore one should notice from Eq. (1) that, although the electronic interaction of quantum wells is neglected, the electromagnetic interaction among them is included via the propagating part of the Green's function.

By inserting into Eq. (1) the explicit expressions for the conductivity response tensor given in Eqs. (3) and (4) one finds that the local field takes the form

$$E_x^{(n)}(z)=E_{0x}(z)+\sum_{m=1}^{N}[a(\omega)F_{xx}^{(m)}(z)\Gamma_x^{(m)}+b(\omega)F_{xz}^{(m)}(z)\Gamma_z^{(m)}] , \tag{8}$$

and

$$E_z^{(n)}(z)=E_{0z}(z)+\sum_{m=1}^{N}[a(\omega)F_{zx}^{(m)}(z)\Gamma_x^{(m)}+b(\omega)F_{zz}^{(m)}(z)\Gamma_z^{(m)}] , \tag{9}$$

where

$$a(\omega)=\frac{\mu_0e^2}{\pi\hbar^2}\frac{(\epsilon_2-\epsilon_1)(\epsilon_F-\epsilon_1)^2}{[\hbar(\omega+i/\tau)]^2-(\epsilon_2-\epsilon_1)^2} , \tag{10}$$

$$b(\omega)=\frac{\mu_0e^2}{2\pi m^*}\frac{(\epsilon_2-\epsilon_1)(\epsilon_F-\epsilon_1)}{[\hbar(\omega+i/\tau)]^2-(\epsilon_2-\epsilon_1)^2} , \tag{11}$$

$$F_{xx}^{(m)}(z)=\int_{(m)}G_{xx}(z,z')\phi^{(m)}(z')dz' , \tag{12}$$

$$F_{xz}^{(m)}(z)=\int_{(m)}G_{xz}(z,z')\Phi^{(m)}(z')dz' , \tag{13}$$

$$F_{zx}^{(m)}(z)=\int_{(m)}G_{zx}(z,z')\phi^{(m)}(z')dz' , \tag{14}$$

$$F_{zz}^{(m)}(z)=\int_{(m)}G_{zz}(z,z')\Phi^{(m)}(z')dz' , \tag{15}$$

$$\Gamma_x^{(m)}=\int_{(m)}\phi^{(m)}(z'')E_x^{(m)}(z'')dz'' , \tag{16}$$

and

$$\Gamma_z^{(m)}=\int_{(m)}\Phi^{(m)}(z'')E_z^{(m)}(z'')dz'' . \tag{17}$$

It is evident from Eqs. (8) and (9) that in order to obtain the final result for the local-field distribution inside the quantum wells the so-far-undetermined quantities $\Gamma_x^{(n)}$ and $\Gamma_z^{(n)}(n=1,2,\ldots,N)$ need to be calculated. To do so, we multiply both sides of Eqs. (8) and (9) by $\phi^{(n)}(z)$ and $\Phi^{(n)}(z)$, respectively, and integrate the resulting equations over z across the nth quantum well. It immediately follows that the $2N$ unknowns $\Gamma_x^{(n)}$ and $\Gamma_z^{(n)}$ can be uniquely determined from the following $2N$ linear inhomogeneous algebraic equations:

$$\Gamma_x^{(n)}-\sum_{m=1}^{N}[a(\omega)K_{xx}^{(n,m)}\Gamma_x^{(m)}+b(\omega)K_{xz}^{(n,m)}\Gamma_z^{(m)}]=S_x^{(n)} , \tag{18}$$

$$\Gamma_z^{(n)}-\sum_{m=1}^{N}[a(\omega)K_{zx}^{(n,m)}\Gamma_x^{(m)}+b(\omega)K_{zz}^{(n,m)}\Gamma_z^{(m)}]=S_z^{(n)} , \tag{19}$$

where

$$K_{xx}^{(n,m)}=\int_{(n)}\phi^{(n)}(z)F_{xx}^{(m)}(z)dz , \tag{20}$$

$$K_{xz}^{(n,m)}=\int_{(n)}\phi^{(n)}(z)F_{xz}^{(m)}(z)dz , \tag{21}$$

$$K_{zx}^{(n,m)}=\int_{(n)}\Phi^{(n)}(z)F_{zx}^{(m)}(z)dz , \tag{22}$$

$$K_{zz}^{(n,m)}=\int_{(n)}\Phi^{(n)}(z)F_{zz}^{(m)}(z)dz , \tag{23}$$

$$S_x^{(n)}=\int_{(n)}\phi^{(n)}(z)E_{0x}(z)dz , \tag{24}$$

and

$$S_z^{(n)}=\int_{(n)}\Phi^{(n)}(z)E_{0z}(z)dz . \tag{25}$$

When the number of wells is not too large, the algebraic equations in Eqs. (18) and (19) can be solved numerically.

Once the local field inside the quantum wells has been obtained, the optical reflection, transmission, and absorption coefficients of the MQW structure can be easily calculated. To this end we first calculate the complex amplitudes of the reflected and transmitted electric fields. By letting the observation point z be located in space $z<0$

one obtains from Eqs. (8), (9), and (12)–(15) that the amplitude of the reflected field is given by

$$\mathbf{E}^R(0)=(-1,0,-\tan\theta)E_x^R(0) , \tag{26}$$

where

$$E_x^R(0)=\sum_{m=1}^{N}[a(\omega)R_{xx}^{(m)}\Gamma_x^{(m)}+b(\omega)R_{xz}^{(m)}\Gamma_z^{(m)}] , \tag{27}$$

with

$$R_{xx}^{(m)}=\left[\frac{c_0}{\omega}\right]^2\frac{q_\perp}{2i\epsilon^B}\int_{(m)}e^{iq_\perp z'}\phi^{(m)}(z')dz' , \tag{28}$$

$$R_{xz}^{(m)}=\left[\frac{c_0}{\omega}\right]^2\frac{q_\parallel}{2i\epsilon^B}\int_{(m)}e^{iq_\perp z'}\Phi^{(m)}(z')dz' , \tag{29}$$

the wave-vector projection parallel to the surface being

$$q_\parallel=[\epsilon^B(\omega)]^{1/2}(\omega/c_0)\sin\theta .$$

Note that the minus sign appearing in Eq. (26) originates in our convention of the positive direction of the electric-field vector in the xyz coordinate system, cf. Fig. 1. This convention has been used in deriving the Green's function given in Eq. (7).[24]

When the observation point z lies in space $z>(N-1)\Lambda+d$ (cf. Fig. 1), where Λ and d are the spatial period and the well width, respectively, we obtain the following results for the amplitude of the transmitted field:

$$\mathbf{E}^T(0)=(\cos\theta,0,-\sin\theta)E_0+(1,0,-\tan\theta)E_x^T(0) , \tag{30}$$

where

$$E_x^T(0)=\sum_{m=1}^{N}[a(\omega)T_{xx}^{(m)}\Gamma_x^{(m)}+b(\omega)T_{xz}^{(m)}\Gamma_z^{(m)}] , \tag{31}$$

with

$$T_{xx}^{(m)}=\left[\frac{c_0}{\omega}\right]^2\frac{q_\perp}{2i\epsilon^B}\int_{(m)}e^{-iq_\perp z'}\phi^{(m)}(z')dz' , \tag{32}$$

$$T_{xz}^{(m)}=-\left[\frac{c_0}{\omega}\right]^2\frac{q_\parallel}{2i\epsilon^B}\int_{(m)}e^{-iq_\perp z'}\Phi^{(m)}(z')dz' . \tag{33}$$

As a definition, the Fresnel reflection (r_p) and transmission (t_p) coefficients of the MQW structure are given by[25]

$$r_p=-E_x^R(0)/(E_0\cos\theta) , \tag{34}$$

and

$$t_p=1+E_x^T(0)/(E_0\cos\theta) . \tag{35}$$

Thus the energy absorption coefficient (absorbance) is defined as

$$A_p=1-|r_p|^2-|t_p|^2 . \tag{36}$$

B. Infinite-barrier approximation: Analytical result

As has been discussed in the preceding section, to calculate the energy absorption coefficient of a MQW structure having N wells one has to solve $2N$ linear algebraic equations. This immediately means that one needs to calculate $2N\times 2N$ matrix elements ($K_{xx}^{(n,m)}$, $K_{xz}^{(n,m)}$, $K_{zx}^{(n,m)}$, and $K_{zz}^{(n,m)}$). Since each element is determined by a double integration [cf. Eqs. (20)–(23)], it is apparent that a purely numerical calculation takes a lot of computer time. In order to facilitate the calculation, it is desirable to obtain analytical expressions for these elements. To this purpose, in the following, we shall adopt the so-called infinite-barrier approximation with an effective well width.[26] In this approximation, the wave function of a finite-barrier well having a *real* well width L_w is replaced by the infinite-barrier wave function with an effective well width d. The effective width is adjusted so that the eigenenergy of the ground state is equal to that calculated within a finite-barrier model. For a semiconductor quantum well d is usually larger than L_w, since, when the barrier height of the quantum well is finite, the wave functions of the electrons can leak into the barrier region.

By use of the infinite-barrier wave functions[20] and by combining Eq. (7) with Eqs. (12)–(15) and Eqs. (20)–(25), we obtain, after some tedious calculations, the following analytical results:

$$K_{xx}^{(n,m)}=\begin{cases}-\dfrac{c_0^2q_\perp^2d}{2\epsilon^B\omega^2}[X_+ +2iq_\perp d(1+e^{iq_\perp d})X_-^2] , & n=m\\ \dfrac{c_0^2q_\perp^3d^2}{i\epsilon^B\omega^2}[1+\cos(q_\perp d)]X_-^2e^{iq_\perp\Lambda|n-m|} , & n\neq m ,\end{cases} \tag{37}$$

$$K_{xz}^{(n,m)}=-K_{zx}^{(n,m)}=\begin{cases}-\dfrac{3\pi^2c_0^2q_\parallel}{2i\epsilon^Bd\omega^2}[X_+ +2iq_\perp d(1+e^{iq_\perp d})X_-^2] , & n=m\\ -\dfrac{3\pi^2c_0^2q_\parallel q_\perp}{\epsilon^B\omega^2}[1+\cos(q_\perp d)]X_-^2e^{iq_\perp\Lambda|n-m|} , & n\neq m ,\end{cases} \tag{38}$$

$$K_{zz}^{(n,m)}=\begin{cases}\dfrac{5\pi^2c_0^2}{\epsilon^B d^3\omega^2}+\dfrac{3\pi^3c_0^2q_\parallel^2}{2i\epsilon^B q_\perp d^2\omega^2}\left[\dfrac{q_\perp d}{3i\pi}Y+6\pi(1+e^{iq_\perp d})X_-^2\right], & n=m \\ \dfrac{9\pi^4c_0^2q_\parallel^2}{i\epsilon^B\omega^2q_\perp d^2}[1+\cos(q_\perp d)]X_-^2e^{iq_\perp\Lambda|n-m|}, & n\neq m,\end{cases} \tag{39}$$

$$S_x^{(n)}=iq_\perp dE_0\cos\theta(1+e^{iq_\perp d})X_-e^{iq_\perp\Lambda(n-1)}, \tag{40}$$

$$S_z^{(n)}=-\frac{3\pi^2}{d}E_0\sin\theta(1+e^{iq_\perp d})X_-e^{iq_\perp\Lambda(n-1)}, \tag{41}$$

where

$$X_\pm=\frac{1}{9\pi^2-(q_\perp d)^2}\pm\frac{1}{\pi^2-(q_\perp d)^2}, \tag{42}$$

and

$$Y=\frac{1}{9\pi^2-(q_\perp d)^2}+\frac{9}{\pi^2-(q_\perp d)^2}. \tag{43}$$

Finally, from Eqs. (28), (29), (32), and (33) one obtains

$$R_{xx}^{(m)}=\left[\frac{c_0}{\omega}\right]^2\frac{q_\perp^2 d}{2\epsilon^B}(1+e^{iq_\perp d})X_-e^{iq_\perp\Lambda(m-1)}, \tag{44}$$

$$R_{xz}^{(m)}=\left[\frac{c_0}{\omega}\right]^2\frac{3\pi^2q_\parallel}{2id\epsilon^B}(1+e^{iq_\perp d})X_-e^{iq_\perp\Lambda(m-1)}, \tag{45}$$

$$T_{xx}^{(m)}=-\left[\frac{c_0}{\omega}\right]^2\frac{q_\perp^2 d}{2\epsilon^B}(1+e^{-iq_\perp d})X_-e^{-iq_\perp\Lambda(m-1)}, \tag{46}$$

$$T_{xz}^{(m)}=-\left[\frac{c_0}{\omega}\right]^2\frac{3\pi^2q_\parallel}{2id\epsilon^B}(1+e^{-iq_\perp d})X_-e^{-iq_\perp\Lambda(m-1)}. \tag{47}$$

In the next section we shall use Eqs. (18), (19), and (37)–(47) to calculate the absorption spectra of a $GaAs/Al_xGa_{1-x}As$ MQW system.

III. RESULTS AND DISCUSSION

In this section we present detailed numerical calculations of the linear optical absorption spectra of a MQW structure for different parameters such as the sheet electron concentration, the angle of incidence, and the number of wells. In this paper we shall take a typical semiconductor $GaAs/Al_xGa_{1-x}As$ quantum well as a numerical example, although the theory developed above can be applied to other n-type two-level quantum wells. The parameters used in the calculation for this semiconductor structure are given as follows. The real well width is $L_w=100$ Å, and the thickness of the barrier layer is $L_b=100$ Å. Thus the spatial period of the MQW structure is given by $\Lambda=L_w+L_b=200$ Å. For the conduction-band discontinuity V_0 between GaAs and $Al_xGa_{1-x}As$, we have chosen $V_0=300$ meV. Using a square-well potential model with the barrier height V_0 and the well width L_w chosen above, the effective well width d was found to be $d=128.5$ Å, and the eigenenergy separation between the two lowest levels was $\epsilon_{21}\equiv\epsilon_2-\epsilon_1=102.7$ meV. In the calculation an effective mass of the electrons of $m^*=0.0665m_e$ has been used, where m_e is the mass of the free electrons. Since the frequency range of interest in the present work is much higher than the resonance frequencies of the optical phonons for GaAs, we shall neglect the frequency dependence of the dielectric constant of the background medium, and take it to be $\epsilon^B\approx10.0$. For the relaxation time of the electrons associated with the intersubband transition between the two lowest-lying bound states, we have chosen $\tau=0.2$ ps. The Fermi energy for the MQW system is determined from the charge neutrality condition of a single quantum well, since the quantum wells in the structure are assumed to be electronically isolated. Therefore, assuming that only the lowest level (ϵ_1) is occupied, one finds that the Fermi energy in the low-temperature limit ($T\to0$) is determined from[20]

$$\epsilon_F=\epsilon_1+\frac{\pi\hbar^2}{m^*}N_s, \tag{48}$$

where N_s denotes the two-dimensional electron concentration. It is clear from Eq. (48) that the position of the Fermi level relative to the lowest level ϵ_1 can be displaced by varying the impurity-doping concentration in the structure, since the surface density of the electrons in the MQW is proportional to the donor concentration. As will be seen below, a change of the Fermi level leads to a shift of the resonance peak in the absorption spectra.

In Fig. 2 we show the optical absorbance A_p of the MQW structure as a function of the photon energy $\hbar\omega$ for different sheet electron concentrations, i.e., $N_s=0.5\times10^{12}$, 1.0×10^{12}, 1.5×10^{12}, 2.0×10^{12}, and 2.5×10^{12} cm^{-2}. The angle of incidence was $\theta=17.1°$, which is equal to the angle of refraction when light is incident on GaAs from vacuum at the Brewster angle ($\sim73°$), as was usually done in optical absorption experiments.[4–8] The number of wells was $N=100$. It appears from Fig. 2 that for each sheet electron concentration the absorption spectrum exhibits a pronounced resonance peak somewhat above the energy separation ϵ_{21}. As the surface density of the electrons is increased, the absorption peak position is upward shifted. The blueshift of the absorption peak location originates in the local-field resonance associated with the electronic intersubband transition.[20,25] Since the local field inside each quantum well in the MQW structure is not only determined by the current

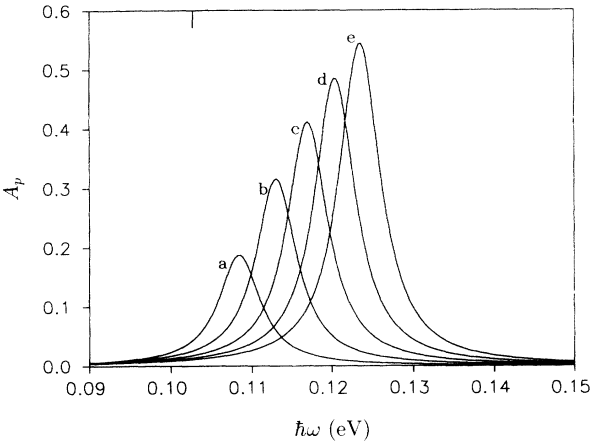

FIG. 2. Optical absorbance A_p as a function of the photon energy $\hbar\omega$ for different surface densities of the electrons (in 10^{12} cm^{-2}): 0.5 (curve *a*), 1.0 (curve *b*), 1.5 (curve *c*), 2.0 (curve *d*), and 2.5 (curve *e*). The tick mark indicates the energy separation ϵ_{21} between the two lowest levels.

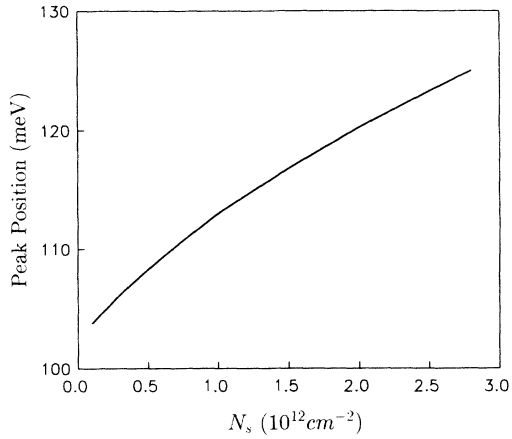

FIG. 3. Peak-position energy in the optical absorption spectra as a function of the surface density of the electrons.

oscillation inside this quantum well driven by the incident field, but also determined by the current flows accompanying the change in the wave function of the electrons between the two levels when the intersubband transition occurs, the resonant optical excitation of the system in general does not take place at the exact energy ϵ_{21}. It happens only when the local field inside the quantum well is resonantly enhanced. The resonance condition is that the determinant of the coefficient matrix of the homogeneous part of Eqs. (18) and (19) is equal to zero. One also notes from Fig. 2 that, as the surface density of the electrons is increased, the maximum absorbance is increased as well. This is to be expected since the current density oscillation of the quantum well increases in magnitude when more electrons are available to contribute. To sustain such strong current oscillation in the quantum well it is required to absorb more photons. By comparing Fig. 2 with Fig. 1 in Ref. 7, one sees that the present local-field calculation qualitatively accounts for the main features of the experimental findings.[7]

In passing, one should stress that in the present theory many-body effects (electron-electron Coulomb interactions and exchange-correlation effects) are not taken into account in the calculation of the electronic properties of the quantum well in the absence of the electromagnetic radiation. It is known that the many-body effects modify the single-particle wave functions and eigenenergies, and hence the energy splitting between the two lowest levels.[7,8,14] As the sheet electron density is increased, the subband splitting tends to either increase or decrease, depending on whether the well or the barrier layers are doped. However, in the range of electron density used in the present calculations, the change in the energy separation due to the many-body effects is expected to be small in comparison to the local-field blueshift.[8]

In Fig. 3 is shown the peak-position energy in the absorption spectra as a function of the two-dimensional density of the electrons, N_s. The number of wells was $N=100$, and the angle of incidence was the same as used in Fig. 2. The maximum value of the surface density of the electrons was chosen so that only the lowest level is occupied. It is quite clear from Fig. 3 that the peak location of the absorption spectra is blueshifted as the surface density of the electrons is increased. A 20-meV relative blueshift in the peak-position energy was found when the surface density of the electrons was increased from 1.0×10^{11} to 2.5×10^{12} cm^{-2}. In comparison with the relative blueshift observed in the experiment[7] the calculated value is somewhat smaller. This may be partly attributed to the neglect of many-body effects in the present calculations.

In Fig. 4 we present the absorbance of the MQW structure having 100 quantum wells as a function of the photon energy for different angles of incidence, namely, $\theta=20°$, 40°, 60°, and 75°. In the calculation a surface electron concentration of $N_s=2.0\times10^{12}$ cm^{-2} was used. One sees from Fig. 4 that the absorption spectrum at a small angle of incidence ($\theta=20°$) reveals an almost symmetric resonance peak around the photon energy $\hbar\omega=120.5$ meV. When the angle of incidence is in-

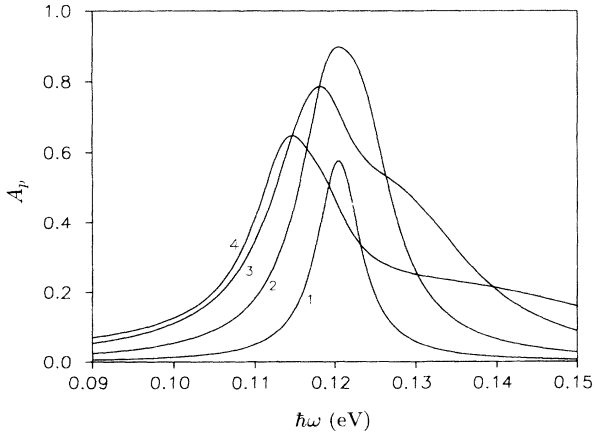

FIG. 4. Optical absorbance A_p as a function of the photon energy $\hbar\omega$ for different angles of incidence, i.e., $\theta=20°$ (curve 1), 40° (curve 2), 60° (curve 3), and 75° (curve 4).

creased, the absorption peak is obviously broadened, and the shape of the absorption spectra in the vicinity of the resonance peak is also changed. The absorption peak becomes more and more asymmetric with an increase in the angle of incidence, and the peak position moves towards the lower energy. The strong angular dependencies of the absorption spectra are attributed to the electromagnetic interaction among quantum wells in the MQW structure. This is so because the local field inside each quantum well is determined not only from the current density oscillation in this well, but also from the current density oscillations of the remaining quantum wells. The coupling among them is included via the propagating part of the electromagnetic Green's function. In addition, one can also see from Fig. 4 that, as the angle of incidence is increased, the optical absorption coefficient first increases and then decreases. This can be more clearly seen from Fig. 5. In this figure we plot the absorption coefficient of the MQW structure as a function of angle of incidence at the photon energy $\hbar\omega = 120.5$ meV. It is evident from Fig. 5 that the optical absorption is very small at small (near 0°) and large (near 90°) angles of incidence ($A_p = 0$ at normal and grazing incidence). In between the two limits a maximum appears around $\theta = 50°$. This is so because, when the angle of incidence is near zero, the z component of the local field almost vanishes, and thus the current density oscillation strength associated with the intersubband transition is very weak [cf. Eq. (41)]. When the light is incident on the MQW structure at large angles of incidence, the incident light is almost totally reflected. Therefore the optical absorption must be very small.

As has been discussed above, the electromagnetic interaction among quantum wells in the MQW structure can lead to a significant broadening of the absorption peak and to a notable change in the shape of the spectra. To illustrate this effect more clearly, we calculated the optical absorption spectra by varying the total number of quantum wells, since one would expect that the more quantum wells contribute, the stronger the electromagnetic coupling among them is. In Fig. 6 are presented the absorption spectra of the MQW structures having 20, 50, 100, and 150 wells, respectively. A surface electron concentration of $N_s = 2.0 \times 10^{12}$ cm^{-2} was employed. The angle of incidence was $\theta = 60°$. It is apparent from Fig. 6 that with an increase in the number of wells the optical absorption is increased, and the shape of the spectra is changed as well. The absorption peak is almost symmetric for the MQW structure having a small number of wells. But it becomes more and more asymmetric when more quantum wells are involved. In addition, as the number of wells is increased, the peak-position energy is downward shifted. From Fig. 6 one also notices that, when the number of wells is larger than 100, an additional small peak, which stems from the resonant local-field interactions in the MQW structure, emerges in the spectra (see curve 4 in Fig. 6). The appearance of the second peak is due to the broadening and distortion of the resonance absorption line as the electromagnetic coupling effects become stronger. This result shows that because of the existence of the strong electromagnetic coupling among quantum wells in the MQW system it is in general difficult to interpret the peaks appearing in the absorption spectra simply as being due to the intersubband transitions.

Before closing the present section, let us address the issue that the electromagnetic interactions in the MQW structure become important only when the following two conditions are satisfied: (i) the local field has a large z component, since the intersubband transition is excited only by this component of the local field, and (ii) the local field within the barrier layers is a propagating wave along the z axis, i.e., the perpendicular component of the wave vector $q_\perp$ is real (the imaginary part of $q_\perp$ must be small if the background medium possesses weak absorption). The first condition requires that the angle of incidence be large [cf. Eq. (41)]. The second condition stems from the fact that the coupling coefficient between two quantum wells is proportional to $\exp(iq_\perp l)$, where l denotes the distance between the two quantum wells [cf. Eqs. (37)–(39)]. Therefore one can easily see that in the electrostatic limit ($c_0 \to \infty$), or in the case where the in-plane component of the wave vector $q_\parallel$ is much larger than

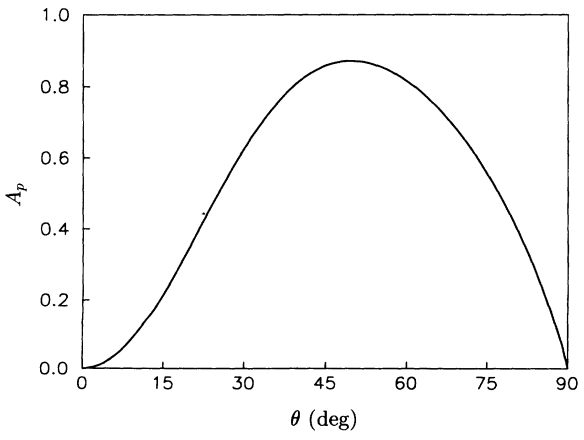

FIG. 5. Angular dependence of the optical absorbance at the photon energy $\hbar\omega = 120.5$ meV.

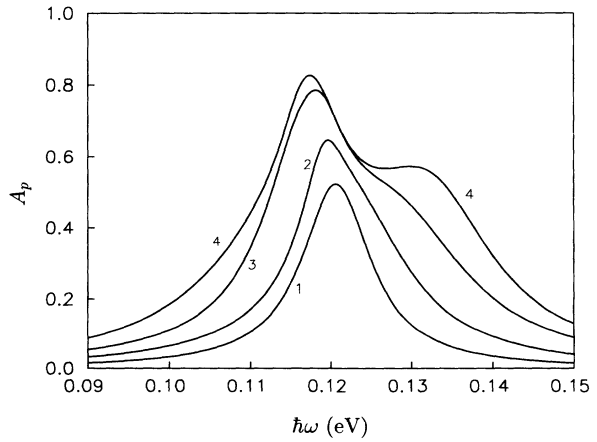

FIG. 6. Optical absorbance A_p as a function of the photon energy $\hbar\omega$ for different numbers of wells, namely, $N = 20$ (curve 1), 50 (curve 2), 100 (curve 3), and 150 (curve 4).

$(\omega/c_0)[\epsilon^B(\omega)]^{1/2}$, $q_\perp \rightarrow +iq_\parallel$, and hence the coupling coefficient decays exponentially with an increase in the distance l. The electromagnetic coupling effects, therefore, are weak in this case. In the previous optical transmission experiments,[4-8] the light was incident directly from vacuum onto the MQW structure, and so the refraction angle (corresponding to the angle of incidence in the present work) is usually small even when the incident angle is equal to the Brewster angle for the vacuum/GaAs system ($\sim 73°$), as was used in experiment.[4-8] Therefore, in order to observe strong electromagnetic coupling in the MQW structure, it is desirable to increase the internal angle of incidence by use of other experimental configurations.

IV. SUMMARY

In the present paper the local-field effect on the linear optical absorption coefficient of a MQW structure in connection with intersubband transitions has been investigated. By neglecting the wave-function overlap between quantum wells, but taking into account the electromagnetic interaction among them, the linear optical absorption coefficient of the MQW structure having only two bound states is derived from a self-consistent integral equation for the local field. Numerical calculations of the optical absorption spectra of a $GaAs/Al_xGa_{1-x}As$ MQW structure are presented for different angles of incidence and numbers of quantum wells. The results show that the local-field effect leads to a significant blueshift of the absorption peak compared with the energy separation between the two levels as the two-dimensional density of the electrons is increased. In the case where the angle of incidence is around 50°, and the number of wells is sufficiently large, the electromagnetic coupling among quantum wells was found to be of importance. Our numerical results demonstrate that the electromagnetic interaction can give rise to a significant broadening of the absorption peak and to a notable change in the peak-position energy and the shape of the spectra.

[1] R. Sooryakumar, A. Pinczuk, A. Gossard, and W. Wiegmann, Phys. Rev. B **31**, 2578 (1985).
[2] A. Pinczuk and J. M. Worlock, Surf. Sci. **113**, 69 (1982).
[3] G. Abstreiter, R. Merlin, and A. Pinczuk, IEEE J. Quantum Electron. **QE-22**, 1771 (1986).
[4] L. C. West and S. J. Eglash, Appl. Phys. Lett. **46**, 1156 (1985).
[5] A. Harwit and J. S. Harris, Jr., Appl. Phys. Lett. **50**, 685 (1987).
[6] B. C. Covington, C. C. Lee, B. H. Hu, H. F. Taylor, and D. C. Streit, Appl. Phys. Lett. **54**, 2145 (1989).
[7] M. O. Manasreh, F. Szmulowicz, T. Vaughan, K. R. Evans, C. E. Stutz, and D. W. Fischer, Phys. Rev. B **43**, 9996 (1991).
[8] B. Jogai, M. O. Manasreh, C. E. Stutz, R. L. Whitney, and D. K. Kinell, Phys. Rev. B **46**, 7208 (1992).
[9] A. Pinczuk, S. Schmitt-Rink, G. Danan, J. P. Valladares, L. N. Pfeiffer, and K. W. West, Phys. Rev. Lett. **63**, 1633 (1989).
[10] M. Ramsteiner, J. D. Ralston, P. Koidl, B. Dischler, H. Beibl, J. Wagner, and H. Ennen, J. Appl. Phys. **67**, 3900 (1990).
[11] Y. Shakuda and H. Katahama, Jpn. J. Appl. Phys. **29**, L552 (1990).
[12] H. Ehrenreich and M. Cohen, Phys. Rev. **115**, 786 (1959).
[13] A. C. Tselis and J. J. Quinn, Phys. Rev. B **29**, 3318 (1984).
[14] G. Eliasson, P. Hawrylak, and J. J. Quinn, Phys. Rev. B **35**, 5569 (1987).
[15] J. K. Jain and S. Das Sarma, Phys. Rev. B **36**, 5949 (1987).
[16] V. A. Shchukin and K. B. Efetov, Phys. Rev. B **43**, 14 164 (1991).
[17] W. Que, G. Kirczenow, and E. Castaño, Phys. Rev. B **43**, 14 079 (1991).
[18] A. Liebsch, J. Phys. C **19**, 5025 (1986).
[19] O. Keller, in *Studies in Classical and Quantum Nonlinear Optics*, edited by O. Keller (Nova Science, New York, 1994).
[20] A. Liu and O. Keller, Phys. Rev. B **49**, 13 616 (1994).
[21] See, e.g., A. Bagchi, Phys. Rev. B **15**, 3060 (1977).
[22] O. Keller and A. Liu (unpublished).
[23] J. E. Sipe, J. Opt. Soc. Am. B **4**, 481 (1987).
[24] O. Keller, Phys. Rev. B **37**, 10 588 (1988).
[25] A. Liu and O. Keller, Phys. Lett. A **177**, 441 (1993).
[26] D. Ahn and S. L. Chuang, IEEE J. Quantum Electron. **QE-23**, 2196 (1987).